Proc. Natl. Acad. Sci. USA
Vol. 96, pp. 5360–5365, May 1999
Astronomy

Intergalactic cold dust in the NGC 4631 group

N. NEININGER*†‡ AND M. DUMKE†§

*Radioastronomisches Institut der Universität Bonn, Auf dem Hügel 71, D-53121 Bonn, Germany; †Institut de Radioastronomie Millimétrique, 300, Rue de la Piscine, F-38406 St. Martin d'Hères, France; and §Max-Planck-Institut für Radioastronomie, Auf dem Hügel 69, D-53121 Bonn, Germany

Edited by Marshall H. Cohen, California Institute of Technology, Pasadena, CA, and approved April 2, 1999 (received for review March 5, 1999)

ABSTRACT **We have detected extraplanar cold dust at distances out to >10 kiloparsecs, situated in the halo of the interacting galaxy NGC 4631. The dust emission disk is much thinner than the warped HI disk, and new structures emerge. In particular, a giant arc has been found that is linked to anomalies in the kinematical structure of the atomic gas. Most of the extraplanar dust is closely associated with HI spurs that have been found earlier [Weliachew, L., Sancisi, R. & Guélin, M. (1978) *Astron. Astrophys.* 65, 37–45; Rand, R. J. (1994) *Astron. Astrophys.* 285, 833–856]. These spurs obviously are traces of the interaction [Combes, F. (1978) *Astron. Astrophys.* 65, 47–55]. The dust emission within the plane reaches the border of the optical disk. The activity of the disk of NGC 4631 is moderately enhanced by the interaction, but no gas moving in the *z*-direction could be found [Rand, R. J., Kulkarni, S. R. & Hester, J. J. (1992) *Astrophys. J.* 396, 97–103; Golla, G., Dettmar, R.-J. & Domgörgen, H. (1996) *Astron. Astrophys.* 313, 439–447]. Hence, it seems unlikely that strong winds have deposited the high-*z* dust. Instead, the coincidence with the HI features suggests that we see a track left behind by the interaction. In addition, the HI shows a supershell formed by an impact [Rand, R. J. & Stone, J. M. (1996) *Astron. J.* 111, 190–196] in the zone where the dust trail crosses the disk. This region is also characterized by disturbances in the distribution of the Hα light. The masses associated with the dust can be estimated only very roughly on the basis of the existing data; they are of the order of a few 10^9 $M_\odot$ of gas.**

Cold dust has come into focus only recently because it had to await the development of sensitive millimeter/submillimeter bolometer arrays to be detectable unambiguously. The Infrared Astronomical Satellite (IRAS) survey could provide only hints at its existence because it was blinded by the strong emission from the small percentage of warmer dust that is radiating far more brightly. The large amount of cold dust ($T_d \leq 25$ K) can be detected only at (sub)mm wavelengths, where the radiation of the warmer components has vanished. To give an example: The peak brightness of a blackbody at 30 K is 30× higher than that of a 15-K object, all other parameters being equal. On the other hand, the radiation of a blackbody at 15 K peaks at ≈200 μm and remains more than one order of magnitude brighter at λ 1.2 mm than that of a blackbody at 30 K with the same peak brightness. Now, the emissivity of interstellar dust is roughly proportional to T_d^6—for a blackbody $B(T) = \sigma T^4$—so even a very large amount of cold dust emits only weakly. Because of this T^6 dependence of the emission, a very large energy input is needed to heat dust, and the majority of it remains at lower temperatures. This cold component thus is an important tracer, and, indeed, it may represent >90% of the interstellar dust (cf. refs. 1 and 2).

In itself, the contribution of the dust to the total mass of a galaxy is <1% of the gas mass, but there are indications that the dust-to-gas ratio is relatively constant, independent of the type of gas (atomic or molecular). Indeed, the dust grains are believed to play a crucial role in the formation of molecules. The study of their properties thus also offers an independent means of studying the molecular gas content of galaxies. This is important because the standard practice of observing the CO molecule and deriving, thereby, the properties of the H_2 has substantial uncertainties, particularly concerning the derived masses. On the other hand, investigating the cold dust is technically difficult and cannot provide any information about the kinematics because it is based on broadband continuum observations.

In several runs, the Institute for Radio Astronomy in the Millimeter domain (IRAM) 30-m telescope equipped with Max-Planck-Institute for Radioastronomy (MPIfR) bolometer arrays has been used to map nearby galaxies in the λ 1.2-mm continuum emission. The first maps led to the impression that it is well correlated with the CO emission and drops off similarly steeply, with increasing distance from the center. This behavior was shown, for example, for galaxies NGC 891 (3), M 51 (4), and NGC 4631 (5). It soon became evident, however, that this is not generally the case. The galaxy NGC 4565 is significantly more extended in the emission of λ 1.2-mm continuum than in that of the CO line (6). The cold dust is even detected in the warped outermost rim of the disk. As an intermediate case, NGC 5907 also shows an extended dust disk (7). The sensitivity needed to detect this extended emission has been achieved only recently, however, and the sample is still small. So it is not yet clear what determines the extent of the cold dust—the profile of the cold dust along the major axis in NGC 891 remains very close to the rapidly vanishing CO, even when studied with much higher sensitivity than previously published (R. Zylka, personal communication).

The Observations and the Object: NGC 4631

Observational Details. All recent maps were obtained with bolometer arrays consisting of 19 elements whose sensitivity is in practice about a factor of 2 better than that of the 7-element detector used before. The 19-element bolometer array has a bandwidth of ≈80 GHz centered at ≈230 GHz. The individual elements are arranged in a closely packed hexagonal pattern. The beam size at the 30-m telescope is 11″, and the spacing between the beams is 20″. The observations were made in March 1997, during a period of stable weather with zenith opacities typically <0.2. We monitored the sky opacity before and after each subimage and mapped Mars every night to determine the absolute flux scale. To obtain a map, the object is scanned in azimuthal direction including parts of blank sky on both sides to define a proper zero level. In addition, the subreflector of the telescope is oscillating at a frequency of 2 Hz, which makes the beam switch between two positions separated by 45″ in the orientation of the scanning. This yields an "on–off" measurement that cancels atmospheric variations at short time scales. The whole area of NGC 4631 was covered

This paper was submitted directly (Track II) to the *Proceedings* office.
Abbreviations: pc, parsec; Jy, Jansky.
‡To whom reprint requests should be addressed. e-mail: nneini@astro.uni-bonn.de.

PNAS is available online at www.pnas.org.

with a mosaic of 19 individual fields. Their distribution is rather uniform along the whole disk and, hence, the sensitivity drops only at the outer edges of the final map. Furthermore, we kept the scanning orientation close to the minor axis of the galaxy by carefully choosing the hour angles of the individual observations. This minimizes spurious contributions and the noise in the map. The field presented here is $\approx 15 \times 8'$ after the cutoff of the edges with lower sensitivity. In the central part, the noise is ≈ 2 mJy/beam (Jy, Jansky) for the data smoothed to an angular resolution of $20''$ and rises to ≈ 3.5 mJy/beam at the edges.

NGC 4631. It is obviously best to choose edge-on galaxies for studies of weak phenomena because the lines of sight are long—remember that the dust emission in the mm regime is optically thin and thus the whole disk contributes to the detectable flux. The 19-element bolometer made it possible to map a large area as well, so we decided to reobserve NGC 4631. This moderately active galaxy has long been a favorite candidate for an interacting system. It is relatively nearby, at 7.5 megaparsecs (Mpc) (ref. 8; $1'$ corresponds to ≈ 2 kpc), and two obvious companions are close by. The dwarf elliptical NGC 4627 is situated $3'$ northwest of the nucleus, and $30'$ to the southeast, the distorted spiral NGC 4656 can be found. The whole group has been extensively studied in HI (8, 9) to understand the traces of the interaction (cf. Fig. 4). According to a modeling of the encounter (10), the prominent streamers of atomic gas can be explained as being pulled out of the members of this group during the interaction. Presumably also as a result of the interaction, the disk of NGC 4631 has a disturbed appearance in the optical continuum and Hα line emission. At two positions in the disk highly energetic "supershells" have been found (11), of which one is described as being caused by the impact of a high velocity object (12).

Almost simultaneously with the early high-resolution HI observations, a large radio halo was detected (13). It is of nonthermal origin and one of the most prominent radio halos known. Detailed investigations (14) have subsequently shown that the magnetic field lines of the galactic disk open into the halo—in stark contrast to most spiral galaxies, where the field is more or less confined in the disk (15). This magnetic field structure allows electrons, cosmic ray particles, and hot gas to escape from the active disk into the halo. ROSAT (Roentgen Satellite) detections (16, 17) show a large x-ray envelope that is a natural consequence of this configuration.

The investigation of the molecular gas indicates rather normal conditions, however. The central region of $\approx 2 \times 1'$ was completely mapped in the (1–0) and (2–1) transitions of CO (18). In addition, a major axis strip of $7'$ length was obtained with a higher sensitivity of ≈ 20 mK. Some additional spectra at other locations did not reveal significant emission.

The Distribution of the Cold Dust

The Dusty Disk. At a first glance, the λ 1.2-mm emission of NGC 4631 (Fig. 1) is characterized by a narrow, extended disk, with a double-peaked central region. About three times weaker than the brightest peaks, at a level of ≈ 30 mJy/beam, the disk is stretched out to a distance of ≈ 13 kpc on either side of the nucleus, gently decreasing in the west, and at a relatively constant level for some 10 kpc in the east (see Fig. 2). This distribution is similar to that found in NGC 4565 (6): The correlation between dust and CO is restricted to the nuclear region whereas the dust in the outer parts of the disk seems to follow the HI. The CO emission drops in a similarly steep manner as the centimetric radio continuum: At a radius of $2.5'$ ($=5.5$ kpc), it has decreased to a tenth of the peak value, and a bit further out, no CO emission could be detected at all. At this radius, the dust emission is still at about one-third of the peak level, however, and it actually stretches out at least to the edge of the optical disk. In fact, the limits are set by the border

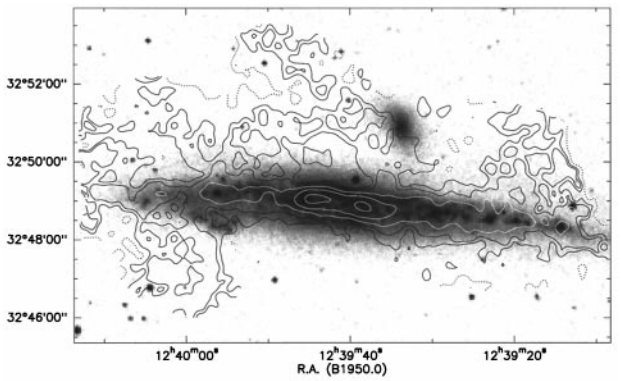

FIG. 1. Map of the λ 1.2-mm emission of NGC 4631, overlaid on an image taken from the Digital Sky Survey. The levels are -6 (dotted), 6, 11, 21, 41, and 81 mJy/beam. Only significant emission is shown, and the outer parts of the map with higher noise have been cut off. The small object north of the disk is the dwarf elliptical galaxy NGC 4627; the other companion, NGC 4656, is situated about half a degree away in the southeast.

of the map, not by the vanishing emission. The old bolometer map (5) is limited to the innermost part due to its restricted coverage and sensitivity.

The narrow main emission ridge is somewhat surprising given the fact that NGC 4631 does not even show a dust lane. Its thickness is similar to that of the undisturbed edge-on galaxies NGC 4565 (6) or NGC 891 (3). This suggests that the dust is concentrated in the midplane of a galaxy, in any case (cf. ref. 19), and the absence of an optical dust lane may just reflect a high clumpiness with large "holes."

A closer inspection shows some radial variations in comparison with the Hα map (Fig. 3). Near the center, the optically bright regions surround the dust emission peaks. Here, the bulk of the optical emission is produced in the central region and later absorbed on its way through the disk. In contrast, in the outer parts of the disk, several dust maxima coincide with optically bright spots. It is unlikely that all of these places are just accidental line-of-sight coincidences. The source of the radiation could be young stars in their dusty birthplaces (e.g., in a spiral arm tangent). In any case, the material along the light path should be rather transparent. Such large variations

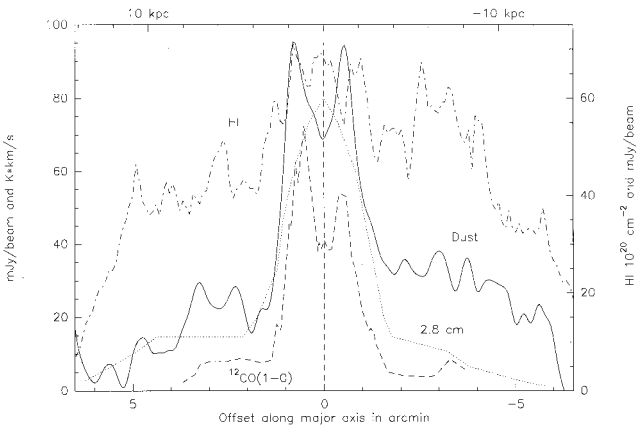

FIG. 2. Cuts along the major axis; the CO and the 2.8 cm data were provided by G. Golla (14, 18), and the HI curve was extracted from a map supplied by R. Rand (8). The left axis gives the units for the dust and CO emission, the right axis for HI and cm continuum. Similar to the galaxies NGC 4565 (6) and 5907 (7), the profiles of the CO and the cm continuum drop off more steeply than that of the dust and the HI. Note, however, that such cuts are one-dimensional and miss emission that is close to, but not on, the major axis.

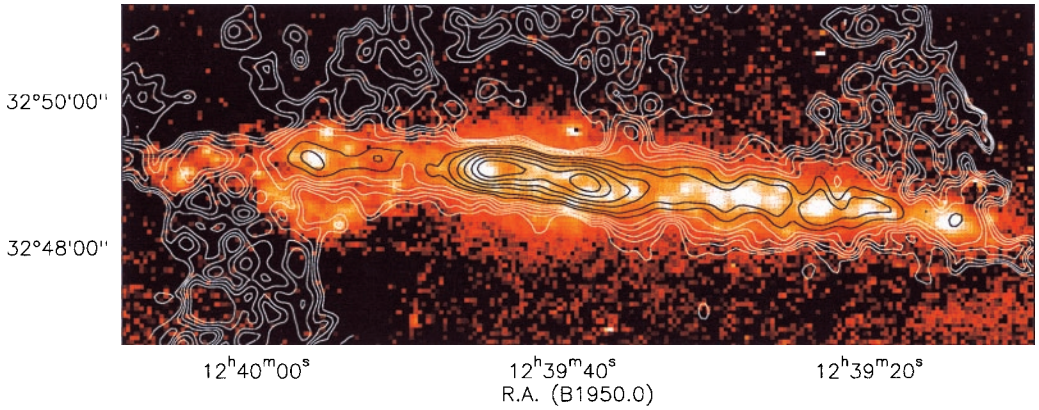

FIG. 3. Comparison of the λ 1.2-mm emission of NGC 4631 with the Hα emission, which has been smoothed to 6″. The dwarf elliptical galaxy NGC 4627 is invisible here. Note the large disturbed area in the west with its subsequent "cutoff." Near the center, the dust and Hα tend to be anticoincident whereas in the outer disk there are clear correspondences.

of the opacity are not surprising for spiral galaxies, however (see ref. 20 for a compilation).

The Extraplanar Dust. Completely new is the detection of significant dust emission out to *z*-distances of at least 10 kpc. The distribution of this intergalactic dust strongly suggests that it has been brought there by the same mechanism that formed the four HI streamers (8, 9). All three HI spurs that are touched by our map are connected with the thin optical disk by corresponding dust features (see Fig. 4). The disk formed by the atomic gas is much thicker than the optical or dust emission disk, however, so that most of the λ 1.2-mm emission still lies within their boundaries. On the other hand, CO emission could only be detected out to $z \approx 1$ kpc. So, either there is hidden molecular gas in those outer regions, or the dust is associated with atomic gas.

Although these streamers follow the already known HI features rather closely, north of the center of NGC 4631, a structure has been unveiled that was invisible in the thick atomic gas disk: A giant arc spans over the central region with its footpoints ≈4 kpc east and west of the central region. The eastern footpoint is situated opposite the onset of the southern streamer 2, and the western part of the arc is blending into spur 4. The thickness of the disk emission seems to be reduced in the central region, but this might be an artifact of the data-

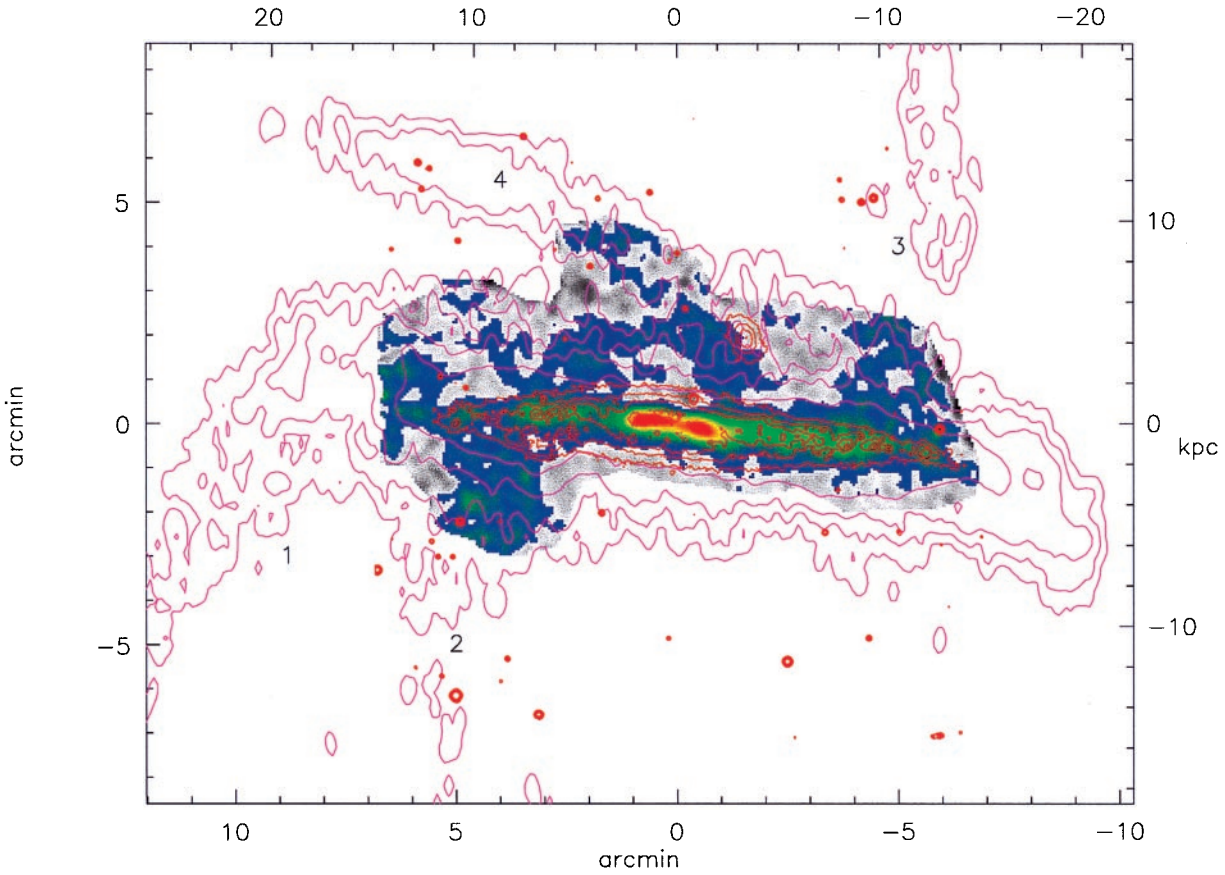

FIG. 4. An overview of the distribution of the extraplanar HI (purple contours) and cold dust (in color); the HI is smoothed to 22″ spatial resolution. For comparison, optical isophotes are added in red. The HI spurs are numbered as introduced in ref. 9. The axis labels are given in arc minutes from the center of NGC 4631 on the lower and left sides; the other sides gives the projected length scale for an assumed distance of 7.5 Mpc.

reducing technique. The question arises regarding whether there is a common origin for these extraplanar structures.

Origin of the Extraplanar Dust

Unfortunately, we do not have any velocity information from the λ 1.2-mm continuum observations and hence have to rely on indirect arguments for the determination of the history of this dust distribution. To some degree, it seems reasonable to assume that the HI velocities are a good indicator also for the dust kinematics. Indeed, there are at least two clear coincidences between HI velocity anomalies and the arc. The velocity gradient along the major axis is much steeper in the northern part of the disk than in the southern. A possible interpretation suggests that the disk is somewhat inclined and warped along the line of sight, so we would be looking at different portions of the galaxy (8)—north of the center at the inner disk with a steeper gradient and south of it at the near part of the outer disk.

If we compare the velocity field with the dust emission (see Fig. 5), a different explanation arises. In addition to the steeper gradient, the northern disk shows anomalous velocity components at two places—and they coincide perfectly with the footpoints of the arc. These anomalous components are visible as regions with almost closed isovelocity contours in Fig. 5 (marked as A1 and A2). Although we are not able to determine the precise location of the extragalactic dust with respect to the disk, it seems clear that there is a local interaction. The additional velocity components point toward us in the west and away from us in the east.

In addition, there are two structural indications, both of them suggesting that material has followed the arc in a counterclockwise direction and hit the disk in the east: (*i*) The appearance of the disk in the light of the Hα line is much more disturbed at the eastern footpoint of the arc (cf. Fig. 3: In broadband red light, the eastern part seems truncated). The disturbed region lies between the arc and the streamer 2 whereas the western side seems unaffected by the arc or streamers 3 and 4. (*ii*) In the HI emission of NGC 4631, two supershells have been found near the midplane and subsequently have been modeled. Shell 2 (west of the nucleus at Right Ascension $12^h39^m30^s$) seems to be an expanding bubble whereas shell 1 (at $12^h39^m56^s$) is most probably caused by an impact of a cloud with a mass of $\approx 10^7\ M_\odot$ at a speed of 200 km/s coming from the north (12). The geometry of the collision is very well constrained by its kinematical signature in the HI data and indicates that the material not only came from the north but, moreover, must have had a velocity component away from us. The location of this shell is between arc and spur 2. This fits to the other indications of the trajectory of the arc (the shells and the anomalous components mentioned above are distinct features).

If we try to describe all extraplanar dust features as a single trail, its path could be as follows: starting from spur 3, it runs through the western disk, follows it to the western footpoint of the arc, sweeps along the arc, penetrates the eastern disk, and leaves it via spur 2. In the way, some material is forced away: for example, to follow streamer 4. Of course, such a concatenation is purely speculative and, at this point, merely meant to summarize the structure of the dust distribution. In principle, the concept of a continuous trail is a natural explanation within the framework of an interaction, however. In any case, we have to answer the question regarding which of the three involved galaxies has left the dust traces.

The interaction has been modeled rather early on the basis of the first high-resolution HI data (10). This description suggests that the bridge 1 and the streamer 4 had been parts of the disk of NGC 4631. The two perpendicular features 2 and 3 are made from material pulled out of the now dwarf elliptical NGC 4627, which might have been of a different type before. However, the HI emission of structures 2 and 3 is only weakly connected with the disk of NGC 4631 and not at all with the dwarf. It has to be stressed that this model is by no means

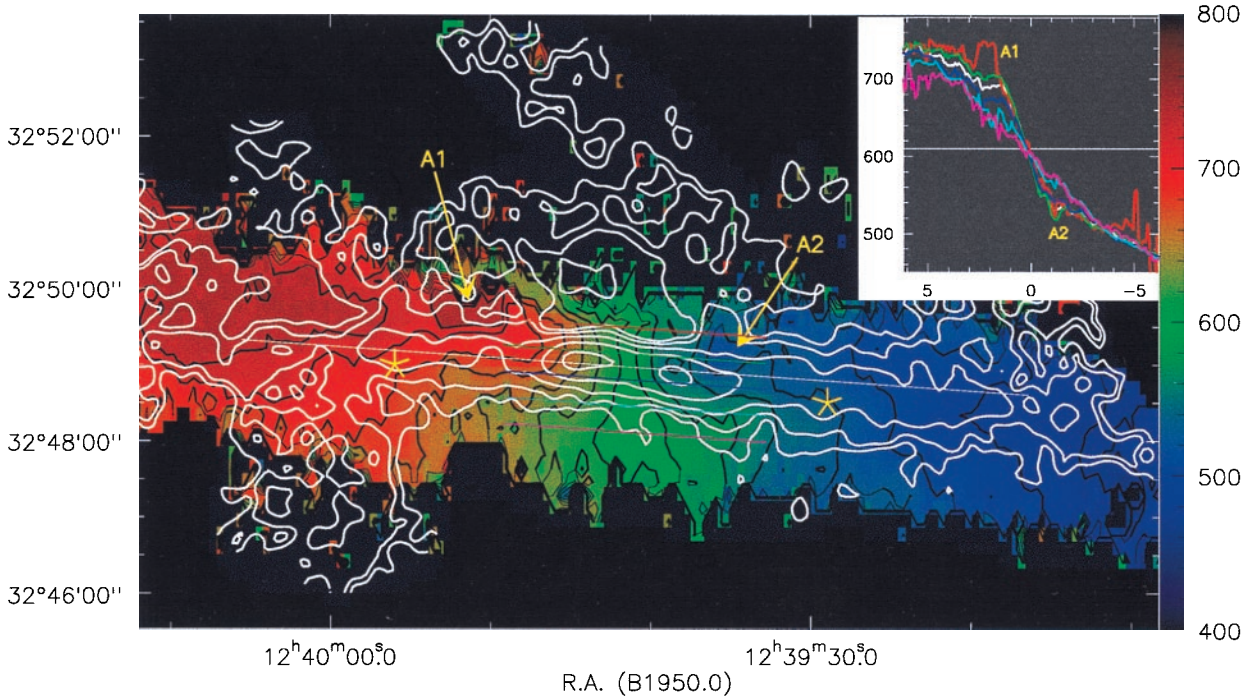

FIG. 5. A comparison between the cold dust emission (at 20″ resolution) and the velocity field of the atomic gas (at 12 × 22″). Velocity contours are plotted every 20 km/s (cf. also the right-hand scale). Note the velocity anomalies at the foot points of the arc (arrows). The insert shows position–velocity curves parallel to the major axis; the box is labeled in velocity vs. minutes of arc. The red line goes through A1, the green line through A2 as indicated by short lines in the main plot. In the southern disk, the gradient is flatter (purple line). The stars mark the position of the two HI supershells.

unique—three involved galaxies open a vast parameter space for an interaction scenario.

Today, the location of part of the HI gas can be determined even in the third dimension with the help of x-ray data: The soft band is very sensitive to absorption by atomic hydrogen, and it can be safely concluded from the distributions that the southern part of the disk is at the near side (16, 17). Looking a bit more in detail, the onset of spur 4 seems to be located in front of the x-ray halo (cf. Fig. 6 of ref. 17), but, higher up, the x-ray emission becomes stronger again, suggesting that this streamer is pointing away from us. Such additional information will help to constrain the parameters of the interaction much better than was possible before.

Discussion and Outlook

Origin of the Millimeter Emission. NGC 4631 is characterized not only by the interaction with two other galaxies but also by an unusually large radio halo. In particular, the enhanced star formation might be responsible for the uncommon magnetic field configuration and thus for the radio and x-ray halo—could this possibly produce extraordinary continuum emission at λ 1.2 mm as well?

In addition to radiation from dust, there are three candidates for the source of radiation: free–free emission in ionized clouds, nonthermal emission, and line radiation within the bandpass of the detector. The free–free emission should be correlated with Hα—so a contribution is only expected in the disk because the sparse high-z Hα emission (21) is not correlated with dust features. Within the disk, even in the brightest spots, the emission measure reaches only a relatively low value of 1,000 pc·cm^{-6} (22). So, the total flux due to free–free radiation is of the order of 10 mJy only.

The synchrotron emission is very extended around NGC 4631 at cm wavelengths (14). From the fluxes and the determined spectral index (23), we can estimate its contribution in our mm band. In the center, the spectral index, is rather flat, at about $\alpha \approx -0.65$. The peak flux here is 60 mJy/84″ beam at 10.55 GHz; this translates into 0.3 mJy/20″ beam at 230 GHz. Outside the disk, the spectral index is even steeper, so this contribution is smaller than a tenth of the noise level. The only significant addition thus comes from the molecular line emission: The eastern peak reaches 70 K·km·s^{-1} of ^{12}CO(2–1) emission. Within our 20″ beam, this contributes to a flux density of ≈20 mJy/beam (cf. ref. 4), about a fifth of the total value. In the outer disk, however, the line emission adds <3 mJy/beam—just the figure of the noise level in the map.

So, the observed mm continuum radiation is pure thermal dust emission almost everywhere, but how did the dust reach such enormous z-heights? Could it simply be blown out of the active plane by large-scale winds? Outflows are known for many galaxies with strong starbursts like, for example, M 82 (see, e.g., refs. 24 and 25). But the disk of NGC 4631 is forming stars at an only moderately enhanced rate (18). Hα kinematic data as a more direct tool do not show signs of a gas outflow from the disk (22)—in contrast to M 82, which has a similar orientation (24). Peculiar velocities have been found, but they are more likely explained by the direct influence of the interaction.

Temperatures and Masses. The dust around the disk of NGC 4631 seems to be cold—the spatially resolved Infrared Astronomical Satellite chopped photometric channel data as an indicator for warmer dust show at most a somewhat thicker disk near the center (26). Its width is of the order of 90″ at 100-μm and 45″ at 50-μm wavelength using the published beam sizes of 95″ and 80″, respectively. No significant emission can be seen further out. Unfortunately, the chopped photometric channel instrument could not be calibrated properly, and, because of the uncertainties of the order of ±60%, we could not derive dust temperatures from these data.

In view of the moderate star forming activity, the presence of very warm material does not seem very likely. Presumably, the temperature of the coldest dust component is rather low even in the disk—similarly to other spirals in which it could be measured so far (2, 6). We expect, therefore, temperatures in the range of 15–20 K for the disk and even lower values for the extraplanar dust. To determine such temperatures, observations in the sub-mm range between 1 mm and 100 μm are needed, but, here, the opaque atmosphere renders them very difficult. This is why only few data of spiral galaxies have been published in this range (e.g., refs. 2 and 27). We will do more observations at λλ 450 μm and 850 μm to complement the existing data. Together, they should provide the spectral information needed for the determination of the temperatures.

Until then, we have to postpone the proper determination of masses and energies from the dust emission. In principle, the dust mass is directly proportional to the detected flux S_λ. With some additional assumptions about the dust and gas properties, we can derive the hydrogen column density. In the millimeter/submillimeter regime, the observed flux density per beam (of half power beam width θ) produced by dust of temperature T_d is given by $S_\lambda = 1.13\,\theta^2\,(1 - e^{\tau\lambda})B(\lambda, T_d)$. Here, $\tau_\lambda = \sigma_\lambda^H$. N_H gives the dust absorption cross section per hydrogen atom, and $B(\lambda,T_d)$ is the Planck law for the radiation of a black body (see ref. 1 for a derivation and ref. 6 for a determination of a possibly typical value). Such a calculation yields $\approx 2 \times 10^9$ $M_\odot$ of hydrogen for the gas associated with a dust component of 21.5 K in the central region (5). As already stated above, the warmer dust radiates much more efficiently, and, hence, a second dust component at 55 K is associated with <1% of this mass (5).

These values are poorly constrained, however, and we face large uncertainties in the temperatures of the coldest component. If we nevertheless assume 15 K for the extraplanar dust, the total gas mass in the arc should be of the order of 1.7×10^9 $M_\odot$, somewhat less than the mass in the central region. A similar value is found for its presumed continuation, spur 2, so that the total gas mass in this structure would be about half of the atomic hydrogen mass of the whole galaxy (8).

Conclusion

Obviously, the interaction is the dominant event in the history of NGC 4631. It has caused a partial disruption of the disk, triggered the star formation activity, provoked an upturned magnetic field configuration, and, last but not least, left trails of atomic gas and dust all around the disk. It is therefore crucial to know exactly how the interaction took place. The existing model (10) was obtained by using a "trial-and-error" method for the parameters. It is virtually impossible to find the proper solution that way; the number of possible parameter sets for an interaction in such a group with three members is simply too large. Moreover, the now existing data (including the distribution of the cold dust) give new and more detailed information to check the model against. The problem is how to explore the parameter space to find the best set. Now there are new, powerful techniques available like so-called "genetic codes" (28), so we hope to obtain a much better view of the interaction, which in turn should help to fix the roots of the related phenomena.

In any case, the detection of cold dust outside of a galactic disk has unveiled the existence of hitherto invisible baryonic matter in the halo region. This will not solve the dark matter problem, even using a favorable estimation of the associated mass, but it is a step toward a more "normal" neighborhood of galaxies—containing less exotic material, probably simpler to understand, but in any case easier to investigate.

We thank G. Golla for the Hα picture and the CO data set, R. Rand for several sets of HI data, A. Vogler for the ROSAT data, and J. Kerp

for help with their interpretation. F. Combes supplied the trajectories for her model so that we got an idea of the time evolution. Part of this work was supported by the Deutsche Forschungsgemeinschaft within the frame of SFB301.

1. Cox, P. & Mezger, P. G. (1989) *Astron. Astrophys. Rev.* **1,** 49–83.
2. Krügel, E., Siebenmorgen, R., Zota, V. & Chini, R. (1998) *Astron. Astrophys.* **331,** L9–L12.
3. Guélin, M., Zylka, R., Mezger, P. G., Haslam, C. G. T., Kreysa, E., Lemke, R. & Sievers, A. (1993) *Astron. Astrophys.* **279,** L37–L40.
4. Guélin, M., Zylka, R., Mezger, P. G., Haslam, C. G. T. & Kreysa, E. (1995) *Astron. Astrophys.* **298,** L29–L32.
5. Braine, J., Krügel, E., Sievers, A. & Wielebinski, R. (1995) *Astron. Astrophys.* **295,** L55–L58.
6. Neininger, N., Guélin, M., García-Burillo, S., Zylka, R. & Wielebinski, R. (1996) *Astron. Astrophys.* **310,** 725–736.
7. Dumke, M., Braine, J., Krause, M., Zylka, R., Wielebinski, R. & Guélin, M. (1997) *Astron. Astrophys.* **325,** 124–134.
8. Rand, R. J. (1994) *Astron. Astrophys.* **285,** 833–856.
9. Weliachew, L., Sancisi, R. & Guélin, M. (1978) *Astron. Astrophys.* **65,** 37–45.
10. Combes, F. (1978) *Astron. Astrophys.* **65,** 47–55.
11. Rand, R. J. & van der Hulst, J. M. (1993) *Astron. J.* **105,** 2098–2106.
12. Rand, R. J. & Stone, J. M. (1996) *Astron. J.* **111,** 190–196.
13. Ekers, R. D. & Sancisi, R. (1977) *Astron. Astrophys.* **54,** 973–974.
14. Golla, G. & Hummel, E. (1994) *Astron. Astrophys.* **284,** 777–792.
15. Dumke, M., Krause, M., Wielebinski, R. & Klein, U. (1995) *Astron. Astrophys.* **302,** 691–703.
16. Wang, Q. D., Walterbos, R. A. M., Steakley, M. F., Norman, C. A. & Braun, R. (1995) *Astrophys. J.* **439,** 176–184.
17. Vogler, A. & Pietsch, W. (1996) *Astron. Astrophys.* **311,** 35–48.
18. Golla, G. & Wielebinski, R. (1994) *Astron. Astrophys.* **286,** 733–747.
19. Xilouris, E. M., Byun, Y. I., Kylafis, N. D., Paleologou, E. V. & Papamastorakis, J. (1999) *Astron. Astrophys.*, **344,** 868–878.
20. Davies, J. I. & Burstein, D. (eds.), (1995) *The Opacity of Spiral Disks* (Kluwer, Dordrecht, The Netherlands), Vol. 469.
21. Rand, R. J., Kulkarni, S. R. & Hester, J. J. (1992) *Astrophys. J.* **396,** 97–103.
22. Golla, G., Dettmar, R.-J. & Domgörgen H. (1996) *Astron. Astrophys.* **313,** 439–447.
23. Golla, G. (1993) PhD Thesis (Univ. of Bonn, Bonn).
24. McKeith, C. D., Greve, A., Downes, D. & Prada, F. (1995) *Astron. Astrophys.* **293,** 703–709.
25. Bregman, J. N., Schulman, E. & Tomisaka K. (1995) *Astrophys. J.* **439,** 155–162.
26. van Driel, W., de Graauw, Th., de Jong, T. & Wesselius, P. R. (1993) *Astron. Astrophys. Suppl.* **101,** 207–252.
27. Alton, P. B., Bianchi, S., Rand, R. J., Xilouris, E. M., Davis, J. I. & Trewhella, M. (1998) *Astrophys. J.* **507,** L125–L129.
28. Theis, Ch. (1999) *Rev. Mod. Astron.*, in press.